Article

Synergic Effect of Nanolignin and Metal Oxide Nanoparticles into Poly(L-lactide) Bionanocomposites: Material Properties, Antioxidant Activity, and Antibacterial Performance

Erlantz Lizundia, Ilaria Armentano, Francesca Luzi, Federico Bertoglio, Elisa Restivo, Livia Visai, Luigi Torre, and Debora Puglia*

Read Online

ACCESS | Metrics & More | Article Recommendations | SI Supporting Information

ABSTRACT: Binary and ternary poly(L-lactide) (PLLA)-based nanocomposites, containing nanolignin (1 wt %) and different metal oxide nanoparticles (0.5 wt %, Ag_2O, TiO_2, WO_3, Fe_2O_3, and $ZnFe_2O_4$), were realized by solvent casting, and their morphological, thermal, surface, optical, antioxidant, and antimicrobial characterizations were performed. The presence of metal oxide nanoparticles at the selected weight concentration affects the surface microstructure of the PLLA polymer, and this outcome is particle-type dependent, according to the shape, morphology, and chemical properties of the selected nanoparticles (NPs). Analogously, wettability of PLLA-based nanocomposites was slightly modified by the presence of hydrophobic lignin nanoparticles and different shaped metal oxides. Results of differential scanning calorimetry (DSC) and X-ray powder diffraction (XRD) tests confirmed that nanoparticle addition confined the mobility of the amorphous phase, increasing at the same time the formation of more numerous but less perfect PLLA crystals. Interestingly, antioxidant activity was also obtained in ternary-based nanocomposites, where a synergic effect of lignin and metal oxide nanoparticles was obtained. Antibacterial tests showed manifest activity of TiO_2 and Ag_2O nanoparticles containing PLLA films, and the time dependence was more evident for *Staphylococcus aureus* than for *Escherichia coli*. Lignin nanoparticles are able to provide protection against UV light while still allowing visible light to pass and even surpass the UV-protection capacity provided by many inorganic nanoparticles. This makes them an attractive renewable additive for the realization of PLLA/metal oxide nanocomposites in the fields of food, drug packaging, and biomedical industry, where antibacterial and antioxidant properties are required.
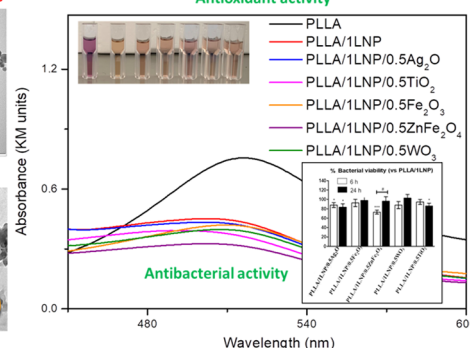
KEYWORDS: *polylactic acid, nanocomposite, metal oxide, lignin, antioxidant, antibacterial*

INTRODUCTION

Polylactic acid (PLA) is a highly potential polymeric material, owing to its exceptional mechanical, transparency, biocompatibility, and biodegradability properties. However, some limitations, such as the narrow processing window due to the high melting temperature and poor thermal stability and limited protection toward many biological, chemical, and physical environmental conditions (physical stress, light, microorganisms, oxygen, and moisture), restrict its complete use in some industrial applications, as in the case of the food packaging sector.[1] In recent times, lignin, as the most abundant natural material after cellulose, has received much interest, due to its multifunctionalities: reinforcement effect, UV protection, and antimicrobial and antioxidation properties.[2] In addition, its use in polylactic acid is considered particularly attractive, being both materials biobased and biodegradable.

There are many examples in the literature of PLA/(micro)lignin systems, where hydrolytic degradation, antioxidant activity, and mechanical properties of PLA/lignin systems have been analyzed, showing, in general, large-sized immiscible areas and impairment of mechanical characteristics, due to the limited compatibility of lignin with polylactic acid.[3] To overcome these limits, different facile and practical routes have been proposed, such as reactive compatibilization,[4] copolymer addition,[5] and filler acetylation.[6]

Quite recently, the introduction of lignin at the nanoscale was also verified to enhance the overall performance of the PLA matrix;[7] some studies already exist offering information about the effect of the inclusion of lignin nanoparticles (LNPs)
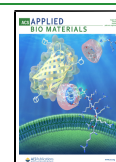
into PLA by different methods. Melt blending, masterbatch procedure, solvent casting, and Pickering emulsion method were considered as suitable methods to incorporate LNPs,[8,9] and the authors evidenced how these nanoparticles could effectively work in improving limited or absent properties in PLA, such as flame retardancy, antioxidant activity, and UV shielding.

Regarding these last specific factors, renewable and biodegradable UV-shielding thin systems are required to meet the pressing sustainable environmental needs, and lignin, as a natural antioxidant and UV blocker, has gained significant consideration.[10] In parallel, UV-blocking additives based on inorganic metal oxide nanoparticles (TiO_2, ZnO, Fe_2O_3)[11,12] have been widely used for these purposes, as their incorporation into different supporting matrices helps reduce the yellowing of their hosting matrix during UV weathering. Inorganic metal oxide nanoparticles are able to absorb UV light but not visible light, making them especially relevant for transparent packaging development.[13] They also have appreciable antioxidant activity.[14] Antimicrobial effects of the same nanoparticles have been also found, as reported in the case of LNPs[15] and nanosized metal oxides.[16]

Furthermore, lignin, as a natural three-dimensional network, has shown the ability to create uniform composite structures with inorganic nanoparticles,[17] so organic−inorganic hybrid materials have similarly received wide-ranging attention. The production of lignin/inorganic nanosystems represents a new methodology for high-value reuse of this material, since the hybridization potentially combines the benefits of all constituents to acquire matching synergic properties. There are a few works regarding the realization of these systems, where emphasis is placed primarily on the chance of using lignin as a precursor for metal oxide synthesis to be further incorporated in polymeric matrices,[18,19] while, to the best of authors' knowledge, limited research is available dealing with the incorporation of lignin nanoparticles,[20] in the presence of other inorganic metal oxide nanoparticles, with the main aim of synergically combining the two nanofillers to enhance UV, antioxidant, and antibacterial protection of the biodegradable polymer matrix.

On the basis of previous results,[12] where the authors developed efficient and cost-effective transparent poly(L-lactide) PLLA films containing different nanofillers/particles to be used in the packaging industry, here we extended the research to the preparation of binary and ternary PLLA-based nanocomposites, realized using both lignin nanoparticles (fixed content at 1 wt %) and different organic nanofillers (content of 0.5 wt % for Ag_2O, TiO_2, WO_3, Fe_2O_3, and $ZnFe_2O_4$). Although here we use commercial metal oxide nanoparticles, the abundant aliphatic hydroxyl groups of lignin provide reducing surfaces for metallic ions into metal oxide nanofillers, potentially reducing the need for environmentally toxic reagents needed during nanoparticle synthesis. Here, we aim to explain how the introduction of organic nanoparticles (NPs) affects the morphological, thermal, and wettability behaviors of PLLA mixed with metal oxides. In the meanwhile, functional properties, such as antibacterial and antioxidant responses of binary and ternary systems, were also investigated.

■ EXPERIMENTAL SECTION

Materials. Polylactic acid (PLLA) with a polydispersity index of 1.27 and molecular weight (M_w) of 120.000 g·mol^{-1} was obtained from Purac Biochem. The titanium(IV) oxide anatase phase (TiO_2)

(<25 nm, 637254-50G), tungsten(VI) oxide (WO_3) (<100 nm, 550086-25G), iron(III) oxide (Fe_2O_3) (<50 nm, 544884-5G), and zinc iron oxide ($ZnFe_2O_4$) (<100 nm, 633844-10G) were supplied from Sigma. Silver oxide nanoparticles (Ag_2O) and P_2O_3 were purchased from Cima NanoTech (Corporate Headquarters Saint Paul, MN). Chloroform was used as a solvent to solution-cast PLLA-based films.

Lignin nanoparticles (LNPs) were extracted from alkali lignin (purchased from Sigma-Aldrich) by a hydrochloric acid process based on the methodology previously published.[21] Specifically, the treatment is based on the stirring of 4% (m/v) lignin in an ethylene glycol suspension for 2 h at 35 °C. Subsequently, hydrochloric acid (8 mL, 0.25 M) was slightly mixed to the solution at the rate of 3−4 drops·min^{-1}; after that, the suspension was stirred again for another 2 h. The material was filtered and then dialyzed in deionized water as long as the solution did not reach the neutral pH.

Nanoparticle Characterization. Metal oxide and lignin nanoparticles were morphologically and chemically characterized. The morphology of the nanoparticles was analyzed by transmission electron microscopy (TEM). A small drop of nanoparticle water dispersion was deposited on a carbon-coated copper grid and analyzed with a JEOL 1200EXII electron microscope (JEOL, Peabody, MA). Micrographs were captured using a SIS VELETA CCD camera (Olympus, Muenster, Germany) equipped with iTEM software.

Fourier transform infrared spectroscopy (FT-IR) analysis was done at room temperature (RT) in the transmission mode on KBr disks using the JASCO FT-IR 615 spectrometer at the wavenumber range 4000−400 cm^{-1}.

Nanocomposite Fabrication. Binary and ternary nanocomposites were prepared by the solution-cast method in chloroform. PLLA (2.5 g) was dispersed in 25 mL of chloroform ($CHCl_3$) and mixed at RT for 4 h. For the realization of PLLA binary films, a specific amount of LNPs (1 wt %) or metal oxide (MO) nanoparticles (0.5 wt %) was dispersed in $CHCl_3$ using a tip sonication in an ice bath (VIBRA CELL Sonics mod. VC 750) for 2 min at 30% amplitude (nanoparticle/$CHCl_3$ ratio was selected at 1 wt %/v).

Polymeric solution and NP suspensions (with the exception of Fe_2O_3) were mixed at RT under a magnetic stirrer for 1 h and then cast. In the case of Fe_2O_3-based films, polymer and metal oxide dispersions were mixed using tip sonication for 2 min at 30% amplitude.

For the preparation of PLLA ternary nanocomposites, LNPs and metal oxide NP suspensions were previously mixed using tip sonication (2 min at 30% amplitude) and added to the PLLA solution; the combination of LNPs and metal oxide NPs was performed following the same procedure reported for the PLLA binary-based films. After complete polymer dissolution, the polymeric solution was then cast on a glass Petri dish (diameter 15 cm) coated with a Teflon substrate and dried at RT and in air for 24 h. The films (thickness of ca. 250 μm) were removed from the Petri dish after drying. The films were positioned in a vacuum oven for 1 week at 40 °C to remove the chloroform still present in the polymeric matrix. The realized formulations are reported in Table 1.

Nanocomposite Characterization. Surface microstructures of the PLLA, binary, and ternary films were analyzed by field emission scanning electron microscopy (FESEM, Supra 25-Zeiss, Germany).

UV−visible (UV−vis) spectroscopy analysis in the transmittance mode was performed with a JASCO V-670 instrument in the 200−900 nm range using a film holder.

Thermal analysis of PLLA films was performed using thermogravimetric measurement (TGA, Seiko Exstar 6000) and carried out as follows: 10 mg weight of samples, nitrogen flow (250 mL·min^{-1}), temperature range from 30 to 900 °C, and 10 °C·min^{-1} heating rate. The thermal degradation temperatures were mainly evaluated and compared.

X-ray powder diffraction (XRD) patterns were obtained using a PANalytical's X'Pert PRO MRD powder diffractometer in the reflection mode using Cu Kα radiation and operating at 45 kV and 30 mA.

Table 1. Formulations for PLLA Binary and Ternary Nanocomposites

material	PLLA (wt %)	LNP (wt %)	MO (wt %)
PLLA	100		
PLLA/1LNP	99	1	
PLLA/0.5ZnFe$_2$O$_4$	99.5		0.5
PLLA/0.5Fe$_2$O$_3$	99.5		0.5
PLLA/0.5WO$_3$	99.5		0.5
PLLA/0.5TiO$_2$	99.5		0.5
PLLA/0.5Ag$_2$O	99.5		0.5
PLLA/1LNP/0.5ZnFe$_2$O$_4$	98.5	1	0.5
PLLA/1LNP/0.5Fe$_2$O$_3$	98.5	1	0.5
PLLA/1LNP/0.5WO$_3$	98.5	1	0.5
PLLA/1LNP/0.5TiO$_2$	98.5	1	0.5
PLLA/1LNP/0.5Ag$_2$O	98.5	1	0.5

Thermal transitions of PLLA films were determined with a Mettler Toledo DSC 822e calorimeter under a nitrogen atmosphere (50 mL·min^{-1}). Samples having 8 ± 1 mg were sealed in an aluminum pan and applying a heating scan from −20 to 220 °C at 10 °C·min^{-1}. The crystalline fraction X_c (%) of the PLLA matrix was calculated as

$$X_c \ (\%) = \frac{\Delta H_f - \Delta H_{cc}}{\Delta H_f^0 \cdot W_m} \times 100 \qquad (1)$$

where ΔH_f and ΔH_c represent the fusion and cold crystallization enthalpies of samples, respectively, and W_m is the PLLA weight fraction in the sample. $\Delta H_f^0 = 106$ J·g^{-1} was considered as the melting heat of an infinitely thick PLLA crystal.[22]

The surface characteristics of PLLA-based films were determined by static contact angle measurements, using the FTA1000 Analyser with the sessile drop method in air with high performance liquid chromatography (HPLC)-grade water. The presence of the different nanoparticles and the surface characteristics of the systems on the wettability properties were evaluated.

Antioxidant Properties. Antioxidant activities of neat PLLA and PLLA binary and ternary systems were estimated using a spectroscopic method.[23] In details, PLLA films (0.1 g) were cut into small pieces, added in 2 mL of methanol, and maintained for 24 h at RT. Methanol solution (1 mL) was added to 1 mL of 2,2-diphenyl-1-picrylhydrazyl (DPPH) in methanol (50 mg·L^{-1}). The methanol solution and extract were maintained at RT in the dark for 60 min. The absorbance was analyzed at 517 nm using a UV spectrometer (Perkin Elmer Lambda 35). The DPPH solution extracted from the neat PLLA film was utilized as the control. The DPPH radical scavenging activity (RSA) was evaluated according to eq 2

$$\mathrm{RSA} \ (\%) = \frac{A_{\mathrm{control}} - A_{\mathrm{sample}}}{A_{\mathrm{control}}} \times 100 \qquad (2)$$

where A_{sample} is the absorbance of different samples and A_{control} is the absorbance of the control.

Bacterial Strains, Culture Conditions, and Antibacterial Assay. The microorganisms used in this study were *Staphylococcus aureus* (ATCC 25923) and *Escherichia coli* (ATCC 25922), kindly supplied by R. Migliavacca (Department of Clinical Surgical, Diagnostic and Pediatric Sciences, University of Pavia, Italy). Both strains were cultured in their appropriate medium: *S. aureus* in brain heart infusion (BHI) (Difco, Detroit, MI) and *E. coli* in Luria Bertani broth (LB) (Difco). They were grown at 37 °C, overnight, under aerobic conditions using a shaker incubator (New Brunswick Scientific Co., Edison, NJ). The bacterial growths were monitored by checking the optical density at 600 nm until reaching a density of 1 × 10^{10} cells·mL^{-1}, determined with a standard curve relating OD$_{600}$ to the cell number.[24] Before carrying out the antibacterial tests, all types of binary and ternary nanocomposite films were sterilized with 70% Et-OH for 10 min and successively washed with sterile dH$_2$O. Later, 200 μL (5 × 10^3) of bacterial suspensions was incubated on films for 6 and 24 h at 37 °C. After the desired incubation time, the viability test was performed through the MTT (3-(4,5-dimethylthiazol-2-yl)-2,5-diphenyltetrazolium bromide; Sigma-Aldrich) assay. The test was performed on the planktonic cell cultures removed after being in contact with the binary and ternary nanocomposite films. The same aliquot of bacteria was inoculated in a tissue culture plate (TCP). Results for binary nanocomposite films were first normalized to TCP and then to plain PLLA films set as 100%. Results for ternary nanocomposite films were first normalized to TCP and then to plain PLLA films and finally to PLLA_LNPs set as 100%. Furthermore, the data for both binary and ternary nanocomposite films were also presented normalized to TCP. The experiments were performed in duplicate and repeated three times. Finally, the results obtained were statistically analyzed using GraphPad Prism 5.0 (GraphPad Inc., San Diego, CA). A Student's unpaired, two-sided *t*-test and one-way variance analysis (ANOVA) were performed. Eventually, multiple comparisons were analyzed with the Bonferroni post hoc test (significance level of $p \leq 0.05$).

■ RESULTS AND DISCUSSION

Nanoparticle Characterization. Particle shape, size, and morphology of the selected nanoparticles were investigated by
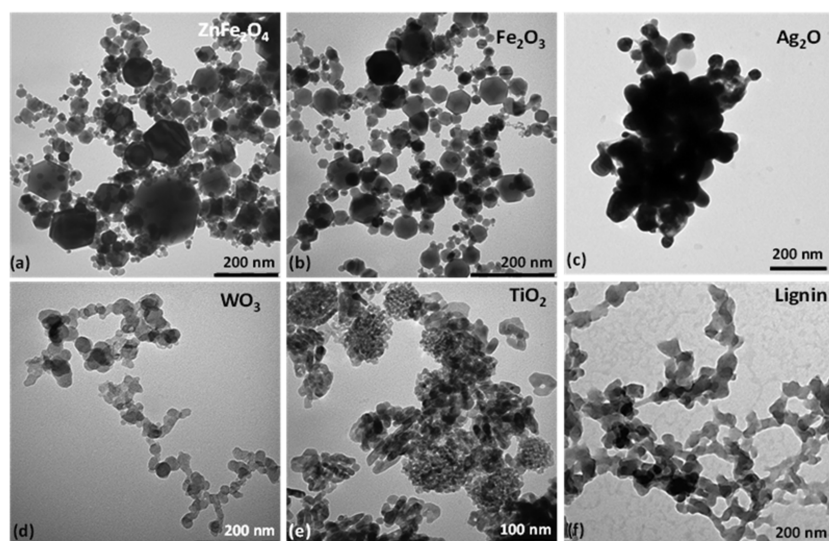

Figure 1. TEM images of metal oxide (a−e) and lignin (f) nanoparticles.

TEM analysis. Figure 1a−e shows images of the as-prepared nanoparticles selected for the binary and ternary nanocomposites, at different resolutions, while in Figure 1f the TEM image of lignin nanoparticles is included. $ZnFe_2O_4$ and Fe_2O_3 nanoparticles have a hexagonal shape with dimensions ranging, respectively, from 20 to 150 nm and from 10 to 100 nm, with a broad distribution in dimension. A spheroid shape was observed in WO_3 nanoparticles, with a narrow size dimension in diameter (20−40 nm). Elongated particles are visible in the TiO_2 sample, with a reduced dimension with respect to other systems. The dimension of Ag_2O nanoparticles ranges around 20−80 nm, and a nanostructured random morphology with particle agglomeration is visible (Figure 1c).

Lignin NPs showed diameters in the range 50 ± 20 nm.[21] Nanoparticles with different morphologies and dimensions were selected. All images highlight the absence of precursor residual material from the synthesis phase, with the exception of Ag_2O, which showed the presence of a surface capping agent used during the production process.[25] The chemical nature of the nanoparticles was confirmed by infrared spectroscopy (Figure S1).

All spectra show the typical infrared signals of inorganic nanoparticles in the low wavenumber regions. $ZnFe_2O_4$ shows two broad adsorption peaks in the range 380−600 cm^{-1}, which is a common characteristic of spinel ferrite NPs. In the case of Fe_2O_3, the absorption peaks at 550, 580, 630, and 680 cm^{-1} are assigned to the stretching vibration mode of Fe−O bonds.[26] Tungsten oxide NPs show the vibration of W−OH and W = O at the wavenumbers of about 848 and 914 cm^{-1}, respectively,[27] while TiO_2 NPs show a broad absorption peak at 483 cm^{-1}, due to the Ti−O stretching vibration.[28] The FT-IR spectrum of Ag_2O NPs shows a broad band at 3253 cm^{-1} due to Ag−O−H stretching, while another peak at 1096 cm^{-1} is induced by O−Ag−O vibration of the Ag_2O crystal. The adsorption bands at 1450 and 1562 are attributed to the bending vibration of −OH (due to the presence of moisture), while the two sharp bands with low intensity at 841 and 663 cm^{-1} are attributed to the stretching vibration of Ag−O−Ag and Ag−O, respectively.[29,30]

Nanocomposite Characterization. *Surface Microstructure.* The cast samples were flexible, smooth, and free-standing, with different colors according to the initial color of the selected inorganic NPs, brown in the case of Fe_2O_3 and $ZnFe_2O_4$ NPs, green/blue in the case of WO_3 and AgO_2 NPs, and white in the case of TiO_2 NP binary films (see visual images in Figure 2—top). Figure 2 shows FESEM surface micrographs of binary PLLA films compared at the same resolution with the corresponding film in the presence of lignin nanoparticles. The presence of metal oxide nanoparticles at the selected weight concentration (0.5 wt %) affects the surface microstructure of the PLLA polymer, and this effect is particle-dependent, according to the shape, morphology, and chemical properties of the selected NPs. The images depict that the pristine PLLA film has an even, compacted, and smooth surface with evidence of parallel lines, due to the mold surface morphologies, while the nanocomposite films consist of a rougher surface morphology. The processing conditions and the nanoparticle's presence impact the surface morphology of PLLA and its nanocomposites. Additionally, the solvent effect was clearly evident, since the final morphological surface aspect was affected by the different solubility of PLLA in chloroform when mixed with oxide nanoparticles.[31] As already reported,[32] aggregation of several nanoparticles, evidenced in the cases of
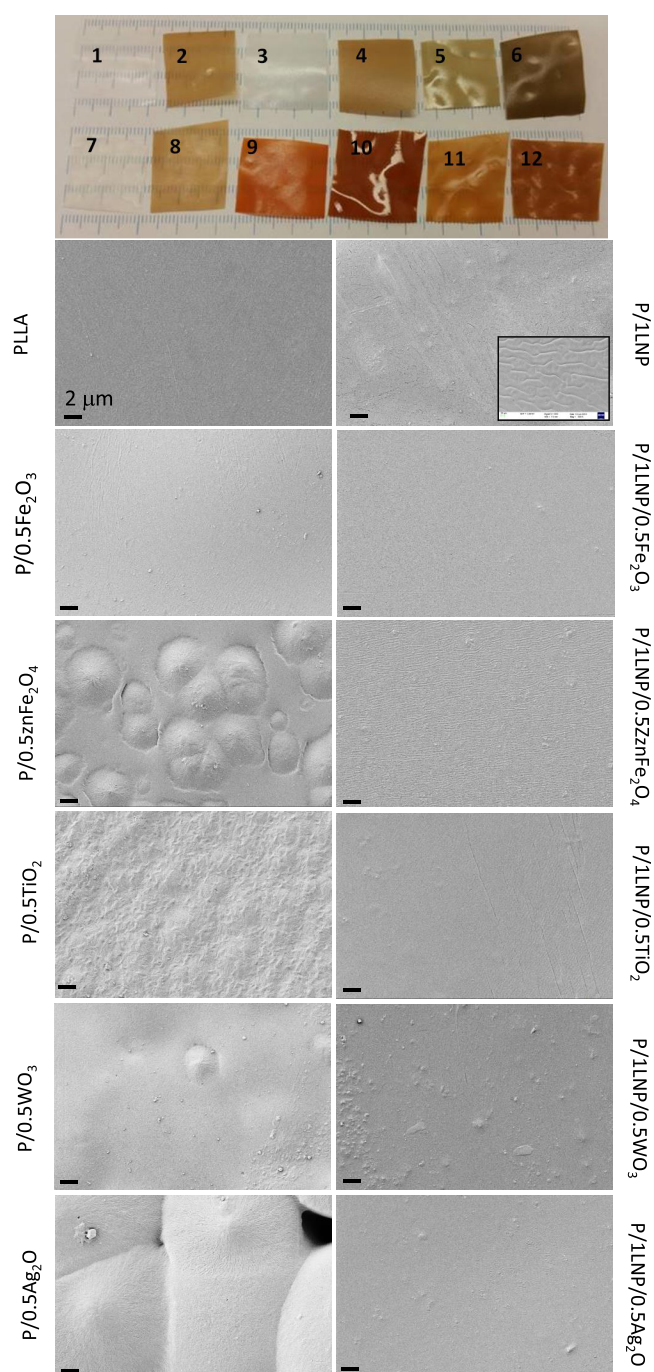

Figure 2. Visual images (1, PLLA; 2, PLLA/1LNP; 3, PLLA/0.5TiO₂; 4, PLLA/1LNP/0.5TiO₂; 5, PLLA/0.5Ag₂O; 6, PLLA/1LNP/0.5Ag₂O; 7, PLLA/0.5WO₃; 8, PLLA/1LNP/0.5WO₃; 9, PLLA/0.5Fe₂O₃; 10, PLLA/1LNP/0.5Fe₂O₃; 11, PLLA/0.5ZnFe₂O₄; 12, PLLA/1LNP/0.5ZnFe₂O₄) and FESEM images depicting the surface microstructure of PLLA ternary films compared with the corresponding PLLA binary films.

ZnO and TiO_2 containing PE films, gave surface morphologies similar to the ones observed here for TiO_2 and $ZnFe_2O_4$. In particular, the incorporation of 0.5 wt % Ag_2O changed the PLLA smooth surface in discrete microphase aggregation (diameter more than 10 μm). Interestingly, it was observed that the addition of LNPs affects the surface properties of the binary nanocomposites. All ternary nanocomposites show a smoother surface, even if the binary corresponding materials

showed a quite rough and controlled microstructure. This effect is particularly marked in silver-based films and also in the case of $ZnFe_2O_4$ NPs. Hence, the different morphologies obtained in the ternary samples could be ascribed to a different interfacial adhesion between the PLLA polymer and metal oxide nanoparticles in the presence of lignin NPs.

Furthermore, we can underline that surface microstructure analysis of both binary and ternary films evidenced no physical defects, like scratches, microcracks, or pinholes, due to solvent evaporation, which suggests successful preparation of the nanocomposites using the solvent casting method.

UV−Vis Spectroscopy. Thanks to their electronic property including a filled valence band and an empty conduction band, many semiconductor nanoparticles such as zinc oxide, titanium dioxide, or iron(III) oxide present a strong UV-absorption tendency.[33] Such inorganic nanoparticles can thus be used as UV-blocking additives to develop films that protect against UV light, which is especially interesting for food packaging applications.[12] Accordingly, nanocomposites were character-ized by UV−vis spectroscopy measurements in the trans-mittance mode. Figure 3 reports the transmittance mode UV−
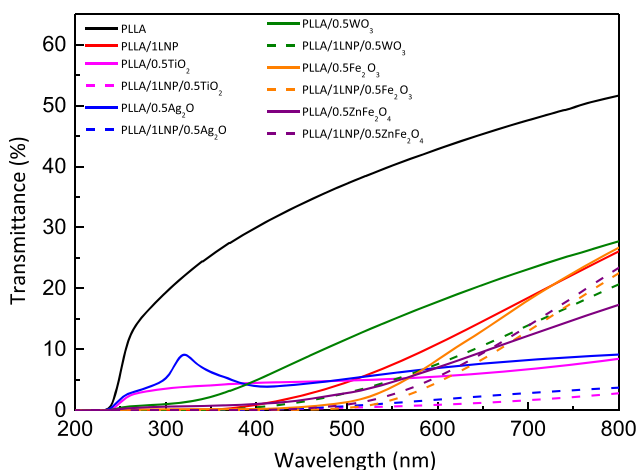
Figure 3. UV−vis transmittance spectra of PLLA binary and ternary films.

vis spectra in the 200−800 nm range (see Table S1 for the amount of transmitted light (%) in the UV region (at $\lambda = 360$ nm) and visible region (540−560 nm)). The neat PLLA film

shows an optical transparency in the 540−560 nm range of 40.2%. Overall, upon nanoparticle addition, such transparency markedly decreases up to a minimum value of 0.6% for the PLLA containing 0.5 wt % TiO_2 and LNPs. The decreased transmittance in the UV region ($\lambda < 400$ nm) provided by the LNPs is noteworthy, which can block almost 100% of the UV light while keeping the optical transparency of the film at 7.5%.

Among inorganic nanoparticles, WO_3 shows a better performance for packaging applications, where as low as possible transmittances at wavelengths below 400 nm and optically transparent films are required.[34] Overall, these results denote that the capacity of lignin nanoparticles to provide protection against UV light while still allowing visible light ($\lambda > 400$ nm) to pass through matches and even surpasses the UV-protection capacity provided by many inorganic nanoparticles, making them an attractive renewable additive to develop materials for food packaging. Interestingly, the UV-screening character of fabricated films may protect the PLLA hosting matrix from photodegradation by absorption of UV radiation and its re-emission in the visible region,[35] providing longer-lasting materials.

TGA Analysis. The thermal performance of PLLA nano-composites has been evaluated by thermogravimetric measure-ments. In Figure 4, derivative thermogravimetric (DTG) curves of binary (a) and ternary (b) PLLA nanocomposites are reported.

As suggested by the bell-shaped curve, the thermodegrada-tion process of PLLA proceeds through a single step (via intramolecular transesterification reactions with the formation of cyclic oligomers),[36] reaching its maximum rate (T_{peak}) at ~362 °C. Despite their high thermal stability, the presence of inorganic nanoparticles decreases the thermal stability of the hosting PLLA matrix as shown by the decrease of T_{peak} up to a minimum of ~327 °C for the PLLA/0.5$ZnFe_2O_4$ nano-composite. This catalyzing effect of inorganic nanoparticles can be ascribed to the fact that nanoparticle surfaces boost depolymerization reactions of adjacent L-lactide units,[36] accelerating the overall thermodegradation process of PLLA.

It has been reported that lignin decomposes through a complex mechanism involving an initial formation of low-molecular-weight elements from cleavage of lignin side chains followed by a methane release due to the cleavage of the main chain (C−C and β−β scission or aryl−ether cleavage) and final condensation of the aromatic structure to lead to char residue.[37] In this sense, it is worth noticing that although the
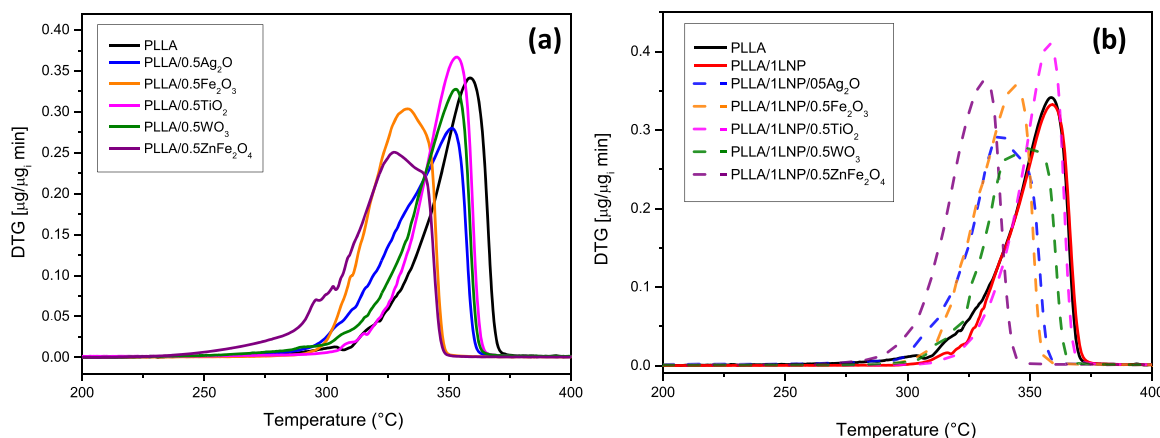
Figure 4. DTG curves of binary (a) and ternary (b) PLLA-based nanocomposites.

thermal stability of ternary nanocomposites is also lower than that corresponding to pure PLLA,[38] it is observed that the addition of lignin can counteract up to a certain extent the marked catalyzing effect of inorganic nanoparticles. The thermal stabilizing effect of lignin is related to the addition of complex phenylpropanoid moieties consisting of aromatic phenyl groups.[3]

XRD Analysis. Powder X-ray diffraction (XRD) measurements were implemented to verify whether or not the incorporation of different nanoparticles (either inorganic or organic) into PLLA could induce changes in the crystalline morphology. Accordingly, Figure 5 shows the XRD patterns on
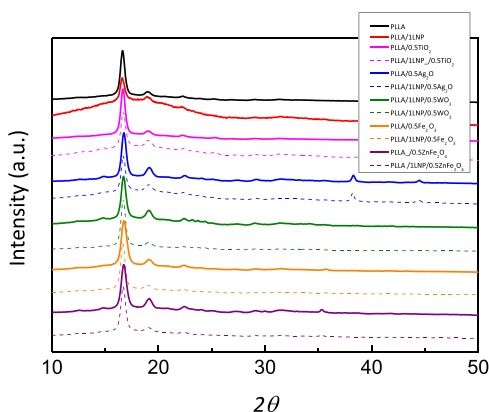

Figure 5. XRD patterns of PLLA binary and ternary films.

nanocomposite films in the 2θ range of 10−50°. The diffraction patterns of all samples are characterized by two main reflections at 2θ of 16.8 and 19.2°, which are ascribed to the (110)/(200) and (203) planes of the α PLLA phase with a 10_3 chain conformation,[39] together with a less intense peak at $2\theta = 22.4°$ arising from the (105) plane. No significant changes in the resulting XRD patterns are observed upon nanoparticle incorporation, indicating that their addition does not modify the crystalline form of PLLA. The size of crystalline domains can be extracted from the most intense (110)/(200) diffraction peak in the XRD patterns according to eq 3[40]

$$\tau = \frac{K \cdot \lambda}{\beta_\tau \cdot \cos \theta} \quad (3)$$

where τ is the average size of the crystals, λ is the wavelength of the incident radiation ($\lambda = 1.5418$ Å), θ is the diffraction angle, K is the Scherrer constant (set at 0.9), and β_τ is the peak width at half-height. As a general trend, the size of crystal domains (see Table S2 for further details) slightly decreases after addition of inorganic nanoparticles, from 17.7 nm for the neat PLLA film to values in the range 14.2−17.4 nm depending on the nanoparticle type. Such smaller sizes can be due to the nucleating effect of nanoparticles, which, acting as heterogeneous nucleation surfaces for PLLA crystallization, yield more but smaller crystals.[41] Additionally, for a given inorganic nanoparticle, the presence of lignin yields crystal size domains comparable to that obtained for neat PLLA, suggesting that lignin nanoparticles limit to a certain extent the nucleating effect of inorganic nanoparticles. We can consider that lignin nanoparticles, especially in solvent cast polymeric films, have limited propensity to induce crystallization. As already observed in our previous work,[8] nucleation effect is improved when homogeneous LNP distribution in the PLA matrix is achieved using the melt extrusion process, while the addition of LNPs at the same concentration (1 wt %) has no effect on the crystallization of the PLA matrix for solvent cast films.

Differential Scanning Calorimetry (DSC) Analysis. Differential scanning calorimetry has been utilized to study the changes induced by nanoparticle addition on the thermal characteristics of PLLA nanocomposites. Accordingly, Figure 6 shows the heating scans of nanocomposite films, while the corresponding main thermal values are reported in Table 2. Neat PLLA is characterized by a smooth enthalpy jump at 34.4 °C arising from the glass transition (T_g) and a marked endothermic peak centered at 179.2 °C corresponding to the melting of its crystals (T_m).[42] The presence of an exothermic peak at intermediate temperatures between T_g and T_m (typically arising from the formation of partial crystallinity during the heating scan), not present in the binary nanocomposite formulations, suggests a relative initially large crystalline fraction of the neat PLLA film (X_c value of 24.5% was obtained for the neat PLLA film).

Binary (Figure 6a) and ternary (Figure 6b) nanocomposites display similar thermograms, where only the transition temperatures were slightly shifted. In this sense, T_g is increased by 3−6 °C depending on the nanoparticle type, suggesting that amorphous PLLA chains are confined by the nanoparticle (either inorganic or organic) surfaces, where the mobility of amorphous segments markedly drops as a result of the
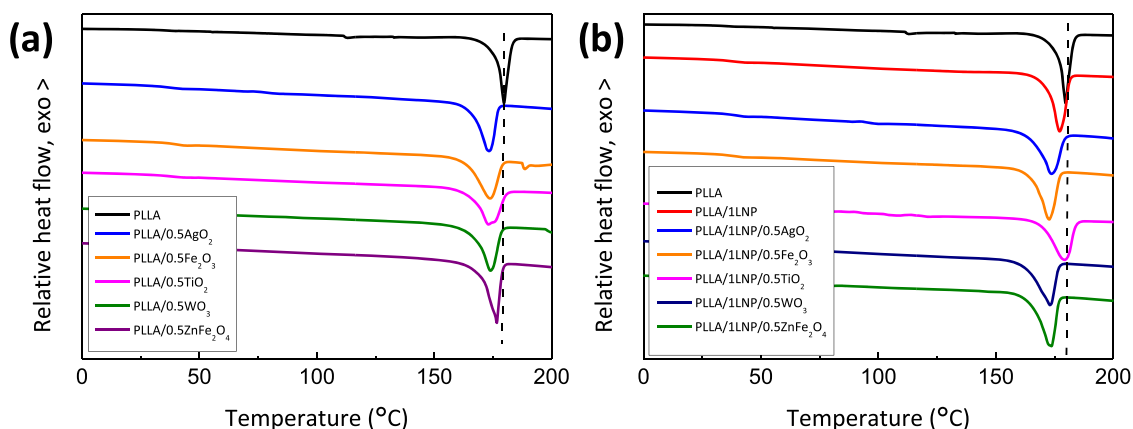

Figure 6. DSC heating curves of PLLA binary (a) and ternary (b) nanocomposites.

Table 2. Thermal Properties Extracted from DSC Analysis (First Heating Scan) for PLLA Nanocomposite Films[a]

formulations	T_g (°C)	X_c (%)	T_m (°C)
PLLA	34.4	25	179.2
PLLA/1LNP	37.0	39	176.7
PLLA/0.5ZnFe$_2$O$_4$	40.4	42	176.1
PLLA/0.5Fe$_2$O$_3$	39.2	44	173.4
PLLA/0.5WO$_3$	37.3	47	173.5
PLLA/0.5TiO$_2$	36.9	41	172.7
PLLA/0.5Ag$_2$O	36.4	47	173
PLLA/1LNP/0.5ZnFe$_2$O$_4$	38.2	42	173.2
PLLA/1LNP/0.5Fe$_2$O$_3$	38.6	44	172.3
PLLA/1LNP/0.5WO$_3$	40.5	45	173.3
PLLA/1LNP/0.5TiO$_2$	38.3	41	177.8
PLLA/1LNP/0.5Ag$_2$O	38.6	46	173.2

[a]T_g, glass-transition temperature; X_c, crystalline fraction; T_m, melting temperature.

attractive forces between the particle surface and the PLLA chains.[43] On the contrary, T_m temperatures decrease from 179.2 °C for pure PLLA to values in the range of 172.3−177.8 °C for the binary and ternary nanocomposites. This behavior may be ascribed to the development of less perfect crystals having thinner lamella, which undergo melting phenomena at lower temperatures.[44]

Moreover, thanks to the effective nucleating behavior of nanoparticles when homogeneously dispersed into a polymer matrix, all nanocomposites present a marked increase in the crystalline fraction in comparison with neat PLLA (from 24.5% for the neat polymer to values in the 38.5−46.5% range).[45] Overall, nanoparticle addition confines the mobility of the amorphous phase while boosting the formation of more numerous but less perfect PLLA crystals.

Wettability. Water contact angle (WCA) is one of the most important and representative parameters to control and study the surface physical characteristics of different films.[46] The static water contact angle (WCA) of nanocomposite surfaces has been determined by the sessile drop methodology, and the obtained values are reported in Figure 7.
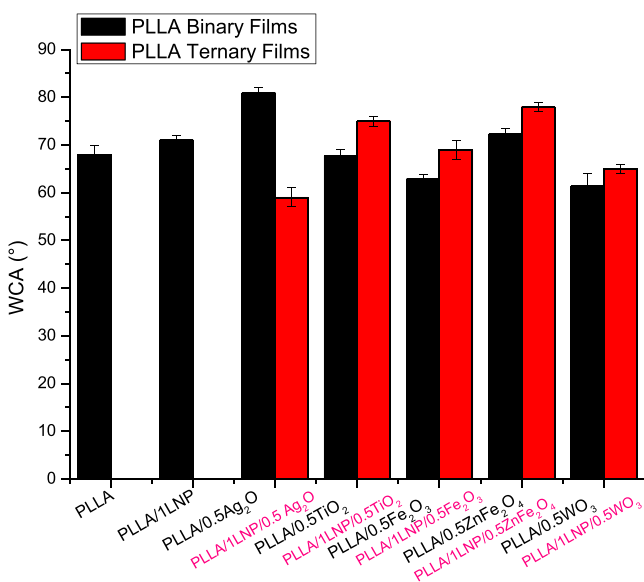
Figure 7. Water contact angles of PLLA binary and ternary films.

The neat PLLA film shows a water contact angle of about 68°.[47] The wettability of PLLA-based nanocomposites is slightly modified in the presence of hydrophobic nanofillers, as in the case of lignin nanoparticles. Specifically, PLLA/1LNP shows increased values of WCA, while a different trend was found for binary systems, according to the different chemical structure, morphology, and dimension of the nanoparticles. The mean value of WCA for PLLA/0.5TiO$_2$ and PLLA/0.5ZnFe$_2$O$_4$ is 68°, almost constant with respect to the PLLA neat film, this trend being in accordance with the literature.[12] A slight decrease is registered for PLLA/0.5WO$_3$; this behavior is related to the low dimension of WO$_3$ nanoparticles as evaluated by the TEM image (Figure 1), which induces a smooth surface in the polymeric matrix (see Figure 2). An increase of 12° for WCA is obtained by the introduction of Ag$_2$O in PLLA, which is caused by the different film surface morphology induced by this formulation (Figure 2). In PLLA/0.5Ag$_2$O binary films, the surface appears with discrete microaggregates, which clearly induces a variation in physical properties. In ternary films, the addition of LNPs induces a variation of water contact angle values in comparison with the same binary films. Generally, a slight increase of WCA is observed in ternary-based films with respect to the binary films, with the exception of PLLA/1LNP/0.5Ag$_2$O, which is characterized by a reduction. This behavior is strongly related to the morphology of the film, since a more smooth and uniform surface (Figure 2) with respect to the binary-based film was observed. As reported by Moradi et al.,[48] surface roughness can cause noteworthy changes in the contact angle values as a function of the characteristics of the asperities in quantity and size,[49] as developed by Cassie's and Wenzel's models, respectively, for hydrophobic and hydrophilic surfaces; thus, wettability can be strongly influenced.[50]

Nanocomposite Antioxidant and Antibacterial Activities. *Antioxidant Properties.* Antioxidant characteristics of PLLA and PLLA/1LNP nanocomposites are determined and expressed as radical scavenging activity (RSA, %). The values of antioxidant activity of migrating extracts in methanol for 24 h for different PLLA-based films are summarized in Table 3,

Table 3. DPPH Scavenging Activity of PLLA Binary and Ternary Nanocomposites

formulations	radical scavenging activity, RSA (%)
PLLA	
PLLA/1LNP	43.1 ± 0.1
PLLA/0.5ZnFe$_2$O$_4$	7.6 ± 0.1
PLLA/0.5Fe$_2$O$_3$	4.2 ± 0.1
PLLA/0.5WO$_3$	3.3 ± 0.3
PLLA/0.5TiO$_2$	6.8 ± 0.1
PLLA/0.5Ag$_2$O	2.4 ± 0.2
PLLA/1LNP/0.5ZnFe$_2$O$_4$	57.6 ± 1.4
PLLA/1LNP/0.5Fe$_2$O$_3$	44.0 ± 2.0
PLLA/1LNP/0.5WO$_3$	48.0 ± 1.1
PLLA/1LNP/0.5TiO$_2$	51.5 ± 1.2
PLLA/1LNP/0.5Ag$_2$O	45.5 ± 0.4

while Figure 8 shows the UV monitoring of the absorbance for the band at 517 nm (Figure 8a) and color difference of the DPPH methanol solution for PLLA/LNP binary and ternary (Figure 8b) systems. LNPs can trap DPPH radicals, a behavior that is confirmed by color change of the DPPH solution from a deep violet to a soft and pale violet color or plate yellow. Metal
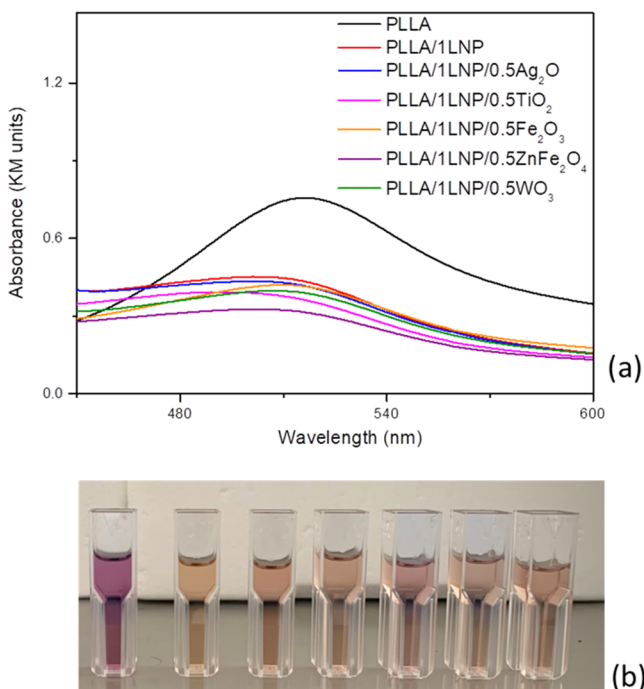
Figure 8. Antioxidant properties of migrated substances for PLLA-based formulations immersed in the methanol solution for 24 h: detection of the absorbance for the band at 517 nm (a), and color modifications of the DPPH methanol mixture (b).

oxide binary-based nanocomposites show antioxidant activity, mainly due to transfer of free electrons from the oxygen atoms present in the nanoparticles to free radicals present at the nitrogen atom of DPPH molecules.[51] Many metal oxide nanoparticles act as antioxidants and scavenge free radicals.

Das et al.[52] found that the RSA activity is largely due to the high surface-to-volume ratio of nanofillers. The PLLA/0.5ZnFe$_2$O$_4$ film shows the highest value of radical scavenging activity among the different metal oxide binary-based nanocomposites (RSA = (7.6 ± 0.1)%).[51] The same trend is also detectable for PLLA ternary-based nanocomposites. The high values of RSA in ternary-based nanocomposites are induced by the presence of natural LNP nanofillers used as antioxidant additives as previously evaluated in a binary-based system (RSA$_{PLLA/LNP}$ = (43.1 ± 0.1)%).[53] The combination of LNP and metal oxide nanoparticles influences positively the RSA response, inducing high values of antioxidant activity (Table 3).

The highest values of RSA in ternary-based systems are registered for PLLA/1LNP/0.5ZnFe$_2$O$_4$ (RSA = (57.6 ± 1.4)%). Also, WO$_3$ and Fe$_2$O$_4$ nanoparticles showed good antioxidant properties; nevertheless, systematic investigations on antioxidant characteristics of ferrite nanoparticles are not available in the literature. The data of our work are promising and offer a lead in the exploration of Fe$_2$O$_4$ and ZnFe$_2$O$_4$ nanoparticles as a new source of antioxidant materials.

Antibacterial Properties. The antibacterial properties of both binary and ternary nanocomposite films were tested by checking the viability of planktonic cell cultures of *S. aureus* and *E. coli* after their removal from the material surface to determine the number of live cells (Figure 9). Figure 9 shows the comparison of *S. aureus* (Figure 9a,c) and *E. coli* (Figure 9b,d) viability on binary (Figure 9a,b) and ternary (Figure 9c,d) nanocomposites at 6 and 24 h, respectively. Considering the times of incubation (6 and 24 h) and the bacterial strains, different results were obtained for binary and ternary nanocomposite films.

Binary-based nanocomposite films showed an interesting antibacterial activity at 6 h in comparison to higher incubation
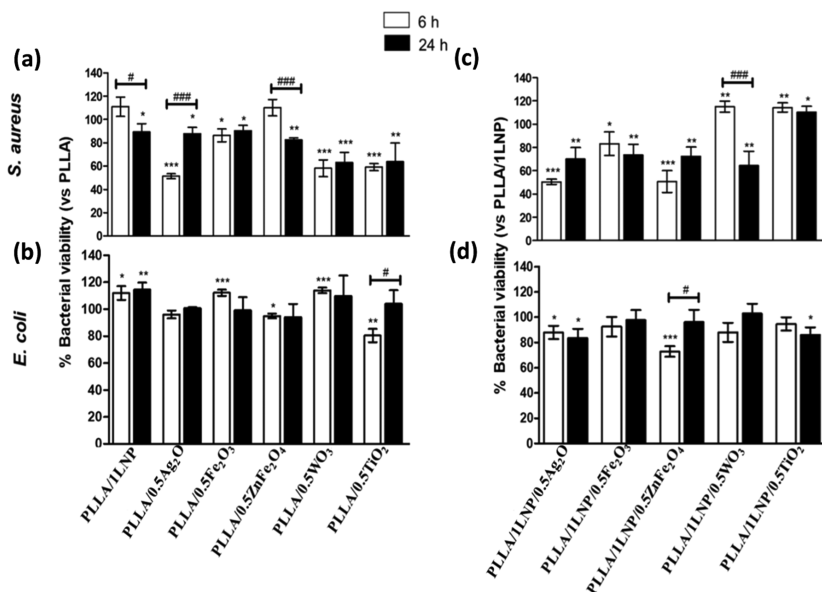
Figure 9. Antibacterial properties of PLLA binary and ternary nanocomposite films on Gram-positive and -negative bacteria. The antibacterial activity was evaluated on the planktonic bacterial cultures removed after being in contact with PLLA and PLLA nanocomposite films containing LNP and/or metal oxide nanoparticles for 6 and 24 h at 37 °C. Results for both binary-based (a, b) and ternary-based (c, d) nanocomposite films, in *S. aureus* (a, c) and *E. coli* (b, d), are expressed as the percentage of bacterial cells grown on the PLLA film set equal to 100% (a, b) or on the PLLA/1LNP film set as 100% (c, d). Data are presented as the average of three replicates ± standard deviations. *, # P < 0,05. *Statistical analysis obtained from Student's *t*-test, normalized vs PLLA (a, b) and vs PLLA/1LNP (c, d); # statistical analysis from ANOVA, followed by Bonferroni's post hoc test for comparison of nanocomposites between 6 and 24 h.

times (24 h) with some differences. Specifically, at 6 h for *S. aureus*, the antibacterial activity trend starting from the higher to the lower value was PLLA/0.5Ag$_2$O (50%) > PLLA/0.5WO$_3$ (~42%) > PLLA/0.5TiO$_2$ (~40%) > PLLA/0.5Fe$_2$O$_3$ (~15%). PLLA/0.5ZnFe$_2$O$_4$ and PLLA/1LNP were not effective on the Gram-positive bacterium (Figure 9a); at 24 h for *S. aureus*, the trend was PLLA/0.5WO$_3$ (~35%) > PLLA/0.5TiO$_2$ (~33%) > PLLA/0.5ZnFe$_2$O$_4$ (~18%) > PLLA/0.5Ag$_2$O (~11%) ≥ PLLA/0.5Fe$_2$O$_3$ ≥ PLLA/1LNP even if the antibacterial activity was relatively reduced on all of the binary nanocomposite films (Figure 9a). For *S. aureus*, the antibacterial activity between 6 and 24 h was quite similar, with the exception of PLLA/0.5Ag$_2$O, which was majorly effective at 6 h, and PLLA/0.5ZnFe$_2$O$_4$, which had an antibacterial activity only after 24 h.

At the short incubation time, *E. coli* showed a different behavior on binary-based nanocomposite films: PLLA/0.5TiO$_2$ (20%) > PLLA/0.5ZnFe$_2$O$_4$ (5%) ≥ PLLA/0.5Ag$_2$O, whereas PLLA/0.5Fe$_2$O$_3$, PLLA/0.5WO$_3$, and PLLA/1LNP did not show any antibacterial activity (Figure 9a). At 24 h for *E. coli*, the trend was slightly different with PLLA/0.5Fe$_2$O$_3$. PLLA/0.5Ag$_2$O and PLLA/0.5ZnFe$_2$O$_4$ showed the best antibacterial performance, maintaining the values observed at 6 h (Figure 9b). For *E. coli*, no significant difference was observed at 6 h when compared with the results at 24 h.

Interestingly, in contrast to our previous studies performed with hydrogels containing the same amount (1 wt %) of lignin nanoparticles (LNPs),[54] the presence of LNPs in PLLA nanocomposite films without metal-based NPs was slightly more effective against the Gram-positive (*S. aureus*) in comparison to the Gram-negative bacteria (*E. coli*) strain; in the latter case, no antibacterial activities were observed. The main reason for the difference may be related to the experimental protocol, which was modified to provide a more accurate understanding on the antibacterial performance: in the previous study, the test was performed directly on the bacteria attached to the material surfaces, whereas in this study, it was detected on the planktonic cell cultures of *S. aureus* and *E. coli* after their removal from the different types of nanocomposite films. Again, we cannot exclude that the different effects could be related to the nature of the PLLA polymer surface induced by the fabrication procedure, as well as LNP distribution in the PLLA films. As shown by the test performed using binary nanocomposite films made of PLLA enriched with metal oxide-based NPs, the antibacterial activity was manifest with PLLA/0.5Ag$_2$O in *S. aureus* and PLLA/0.5TiO$_2$ for both bacterial strains, even if to a different extent. As previously reported, metal oxide nanoparticles, especially TiO$_2$ and Ag$_2$O nanoparticles, demonstrated significant antibacterial activity.[55,56] Within this study, we showed that TiO$_2$ and Ag$_2$O nanoparticles, immersed in a polymer such as PLLA, seem to retain to some extent their antibacterial effect; indeed, it is supported by the Supporting Information Figure S2, whose results were normalized only vs TCP. Interestingly, regarding the other samples tested, PLLA/0.5WO$_3$ showed a better result with *S. aureus*, whereas PLLA/0.5ZnFe$_2$O$_4$ reduced at some level *the E. coli* viability (Figure 9b) and supported by the supplementary figure (Figure S2b). The iron oxide nanoparticles showed therapeutic activities and demonstrated to be efficient antimicrobial agents.[57] These nanoparticles can be used in the treatment of microbial infections because they might function as a membrane permeability enhancer, either causing damages in the cell wall or generating reactive oxygen species. In our study, the antimicrobial activity of iron oxide nanoparticles was better in the presence of zinc ferrite, in particular retaining the antibacterial activity at 6 and 24 h in *E. coli*. As previously reported,[58] zinc nanoparticles were also found to exhibit interesting antimicrobial properties against bacteria, both Gram positive and negative, and fungi. To better explain these results, it is first important to consider that the main toxicological effect induced by metal oxide-based NPs in bacteria occurs by direct contact with the bacteria cell surface. It has been reported that both Gram-positive and -negative bacteria have a negatively charged surface: the cell wall of Gram-positive bacteria is composed of a thick layer of peptidoglycan forming a cohesive mesh, additionally enriched with the external protrusion of the negatively charged teichoic acids (with high levels of phosphate groups). Gram-negative bacteria instead have a thin layer of peptidoglycan and another membrane with partially phosphorylated lipopolysaccharides. The latter increase the negative charge of the surface.[59] Due to electrostatic interactions, positively charged metal-based nanoparticles are attracted by the negatively charged bacterial surface, and their consequent bond causes the disruption of cell walls and the increased permeability. Furthermore, NPs can release metal ions, which can enter the cell to induce the production of reactive oxygen species (ROS) and can interact with cellular structures like proteins, membranes, and DNA, ending with the disruption of cell functions.[59] In this study, we need to consider at least two aspects; (a) the lignin and the metal oxide nanoparticles were not free but included in the PLLA films; and (b) the evaluation was performed on the planktonic cell cultures of both bacterial strains after their removal from the different nanocomposite films at 6 or 24 h. It may be possible that bacterial cells that are in direct contact with the material surface during incubation time can reduce their survivability, whereas those cells that are distant cannot interact directly and hence can survive. Our data seems to confirm the retained effect of some of the inorganic metal oxide nanoparticles even when they are incorporated in PLLA.

Regarding the ternary nanocomposite films, we evaluated the antibacterial performance of PLLA/1LNP containing metal oxide-based nanoparticles to determine in what manner their concurrent presence can effectively reduce bacterial viability. Ternary-based nanocomposite films showed a trend in antibacterial activity quite similar to the one exerted by binary nanocomposite films with some differences (Figure 9c,d). Specifically, at 6 h for *S. aureus*, the antibacterial activity trend starting from the higher to the lower value showed PLLA/1LNP/0.5Ag$_2$O (60%) ≥ PLLA/1LNP/0.5ZnFe$_2$O$_4$ (60%) > PLLA/1LNP/0.5Fe$_2$O$_3$ (40%), whereas no activity was observed for PLLA/1LNP/0.5WO$_3$ and PLLA/1LNP/0.5TiO$_2$ (Figure 9c); at 24 h for *S. aureus*, the trend of the antibacterial activity was relatively different on all of the ternary nanocomposite films: PLLA/1LNP/0.5WO$_3$ (56%) > PLLA/1LNP/0.5Ag$_2$O ≥ PLLA/1LNP/0.5Fe$_2$O$_3$(45%) ≥ PLLA/1LNP/0.5ZnFe$_2$O$_4$ (35%). PLLA/1LNP/0.5TiO$_2$ did not show any antibacterial activity (Figure 9c). For *S. aureus*, the antibacterial activity exerted at 6 h was retained to some extent at 24 h, showing an improvement in particular for PLLA/1LNP/0.5WO$_3$. At 6 h incubation time, the *E. coli* showed a different behavior: PLLA/1LNP/0.5ZnFe$_2$O$_4$ (35%) > PLLA/1LNP/0.5Ag$_2$O (5%) ≥ PLLA/1LNP/0.5WO$_3$ (5%), whereas PLLA/1LNP/0.5Fe$_2$O$_3$ and PLLA/1LNP/0.5TiO$_2$ did not show any efficient activity against bacteria (Figure 9d). At 24 h incubation time for *E. coli*, the trend was slightly

different for PLLA/1LNP/0.5Ag$_2$O and PLLA/1LNP/0.5TiO$_2$ showing the best antibacterial performance even if at quite a low value, whereas no activity was observed on the other ternary nanocomposite films (Figure 9d). For *E. coli*, no great difference was observed at 6 h when compared at 24 h with a slight increment in efficacy exerted by both PLLA/1LNP/0.5Ag$_2$O and PLLA/1LNP/0.5TiO$_2$. In addition, PLLA/1LNP/0.5ZnFe$_2$O$_4$ has an inhibitory effect at 6 h of incubation.

Ternary blends are much more complex multiphase polymeric systems because they can show different microstructures and interactions between polymers, LNPs, and metal oxide nanoparticles. The characteristics of the final products may arise from the different properties of each component of the blend, whereas the various interfacial features could affect the properties of multiphase systems.[60] The interest of ternary nanocomposites is in continuous expansion,[60] and it might be due to the fact that new functional properties could be obtained from the synergy resulting from interfacial interactions of different phases in the blend, thus to be differently influenced. Moreover, the different localization of nanoparticles could influence the morphology and the surface;[60] indeed, they can explain the different behavior in bacterial strains, in accordance with the literature.[61,62]

CONCLUSIONS

Solvent cast films of PLLA-based nanocomposites containing lignin (1 wt %) and different metal oxide nanoparticles (0.5 wt %, Ag$_2$O, TiO$_2$, WO$_3$, Fe$_2$O$_3$, and ZnFe$_2$O$_4$) were prepared and tested determining the thermal, morphological, surface, optical, antioxidant, and antibacterial characteristics. The presence of lignin nanoparticles affected the morphologies of the produced ternary films, as confirmed by the smoother and more hydrophobic surfaces, with the exception of PLLA/1LNP/0.5Ag$_2$O, where the roughness effect was predominant on chemical nanoparticle reactivity. The combined use of metal oxides and lignin also proved effective in UV-protection capacity, surpassing the results obtainable with inorganic nanoparticles. The decreased thermal stability of PLLA upon inorganic NP addition was partially recovered by the stabilizing effect of lignin, while on the other hand, lignin inhibited the nucleating effect of inorganic nanoparticles in the polymer by confining the mobility of the amorphous phase and boosting the formation of more numerous but less perfect PLLA crystals. Interestingly, the presence of metal oxide NPs also corroborates the antioxidant character of the lignin-containing films, which were present in the ternary films and were maximum in ZnFe$_2$O$_4$-based films. Binary nanocomposite films with metal oxide NPs also displayed a significant antibacterial activity against PLLA, more evident for *S. aureus* than *E. coli*, which was maintained only for a few ternary nanocomposite films in a time dependence that was more evident for *S. aureus* than for *E. coli*.

ASSOCIATED CONTENT

Ⓢ Supporting Information

The Supporting Information is available free of charge at https://pubs.acs.org/doi/10.1021/acsabm.0c00637.

Tables showing transmitted light (%), size of the crystalline domains according to the Scherrer equation, FT-IR of metal oxide nanoparticles, antibacterial properties of binary and ternary nanocomposites (PDF)

AUTHOR INFORMATION

Corresponding Author

Debora Puglia − *Civil and Environmental Engineering Department, UdR INSTM, University of Perugia, 05100 Terni, Italy;* ⓘ orcid.org/0000-0001-8515-7813; Email: debora.puglia@unipg.it

Authors

Erlantz Lizundia − *Faculty of Engineering in Bilbao, Department of Graphic Design and Engineering Projects, University of the Basque Country (UPV/EHU), Bilbao 48013, Spain; BCMaterials, Basque Centre for Materials, Applications and Nanostructures, 48940 Leioa, Spain; Laboratory for Multifunctional Materials, Department of Materials, ETH Zürich, 8093 Zürich, Switzerland*

Ilaria Armentano − *Department of Economics, Engineering, Society and Business Organization (DEIM), University of Tuscia, 01100 Viterbo, Italy*

Francesca Luzi − *Civil and Environmental Engineering Department, UdR INSTM, University of Perugia, 05100 Terni, Italy*

Federico Bertoglio − *Molecular Medicine Department, UdR INSTM and Center for Health Technologies, University of Pavia, 27100 Pavia, Italy*

Elisa Restivo − *Molecular Medicine Department, UdR INSTM and Center for Health Technologies, University of Pavia, 27100 Pavia, Italy; Department of Occupational Medicine, Toxicology and Environmental Risks, Istituti Clinici Scientifici Maugeri S.p.A Società Benefit, IRCCS, 27100 Pavia, Italy*

Livia Visai − *Molecular Medicine Department, UdR INSTM and Center for Health Technologies, University of Pavia, 27100 Pavia, Italy; Department of Occupational Medicine, Toxicology and Environmental Risks, Istituti Clinici Scientifici Maugeri S.p.A Società Benefit, IRCCS, 27100 Pavia, Italy;* ⓘ orcid.org/0000-0003-1181-3632

Luigi Torre − *Civil and Environmental Engineering Department, UdR INSTM, University of Perugia, 05100 Terni, Italy*

Complete contact information is available at:
https://pubs.acs.org/10.1021/acsabm.0c00637

Author Contributions

The manuscript was written through contributions of all authors. All authors have given approval to the final version of the manuscript.

Notes

The authors declare no competing financial interest.
All of the data used to support the findings of this study are included within the article.

■ REFERENCES

(1) Bindu, J.; Sathish Kumar, K.; Panda, S. K.; Katiyar, V. In Biopolymer Dispersed Poly Lactic Acid Composites and Blends for Food Packaging Applications BT - Advances in Sustainable Polymers. *Processing and Applications*; Katiyar, V.; Gupta, R.; Ghosh, T., Eds.; Springer: Singapore, 2019; pp 209−235.

(2) Yang, W.; Fortunati, E.; Dominici, F.; Giovanale, G.; Mazzaglia, A.; Balestra, G. M.; Kenny, J. M.; Puglia, D. Synergic Effect of Cellulose and Lignin Nanostructures in PLA Based Systems for Food Antibacterial Packaging. *Eur. Polym. J.* 2016, 79, 1−12.

(3) Gordobil, O.; Delucis, R.; Egüés, I.; Labidi, J. Kraft Lignin as Filler in PLA to Improve Ductility and Thermal Properties. *Ind. Crops Prod.* 2015, 72, 46−53.

(4) Chung, Y.-L.; Olsson, J. V.; Li, R. J.; Frank, C. W.; Waymouth, R. M.; Billington, S. L.; Sattely, E. S. A Renewable Lignin−Lactide Copolymer and Application in Biobased Composites. *ACS Sustainable Chem. Eng.* 2013, 1, 1231−1238.

(5) Sun, Y.; Yang, L.; Lu, X.; He, C. Biodegradable and Renewable Poly(Lactide)−Lignin Composites: Synthesis, Interface and Toughening Mechanism. *J. Mater. Chem. A* 2015, 3, 3699−3709.

(6) Kim, Y.; Suhr, J.; Seo, H.-W.; Sun, H.; Kim, S.; Park, I.-K.; Kim, S.-H.; Lee, Y.; Kim, K.-J.; Nam, J.-D. All Biomass and UV Protective Composite Composed of Compatibilized Lignin and Poly (Lactic-Acid). *Sci. Rep.* 2017, 7, No. 43596.

(7) Tian, D.; Hu, J.; Bao, J.; Chandra, R. P.; Saddler, J. N.; Lu, C. Lignin Valorization: Lignin Nanoparticles as High-Value Bio-Additive for Multifunctional Nanocomposites. *Biotechnol. Biofuels* 2017, 10, No. 192.

(8) Yang, W.; Fortunati, E.; Dominici, F.; Kenny, J. M.; Puglia, D. Effect of Processing Conditions and Lignin Content on Thermal, Mechanical and Degradative Behavior of Lignin Nanoparticles/ Polylactic (Acid) Bionanocomposites Prepared by Melt Extrusion and Solvent Casting. *Eur. Polym. J.* 2015, 71, 126−139.

(9) Chollet, B.; Lopez-Cuesta, J.-M.; Laoutid, F.; Ferry, L. Lignin Nanoparticles as A Promising Way for Enhancing Lignin Flame Retardant Effect in Polylactide. *Materials* 2019, 12, No. 2132.

(10) Xing, Q.; Buono, P.; Ruch, D.; Dubois, P.; Wu, L.; Wang, W.-J. Biodegradable UV-Blocking Films through Core−Shell Lignin−Melanin Nanoparticles in Poly(Butylene Adipate-Co-Terephthalate). *ACS Sustainable Chem. Eng.* 2019, 7, 4147−4157.

(11) Gao, Y.; Gereige, I.; El Labban, A.; Cha, D.; Isimjan, T. T.; Beaujuge, P. M. Highly Transparent and UV-Resistant Superhydrophobic SiO2-Coated ZnO Nanorod Arrays. *ACS Appl. Mater. Interfaces* 2014, 6, 2219−2223.

(12) Lizundia, E.; Vilas, J. L.; Sangroniz, A.; Etxeberria, A. Light and Gas Barrier Properties of PLLA/Metallic Nanoparticles Composite Films. *Eur. Polym. J.* 2017, 91, 10−20.

(13) Wang, H.; Qiu, X.; Liu, W.; Fu, F.; Yang, D. A Novel Lignin/ ZnO Hybrid Nanocomposite with Excellent UV-Absorption Ability and Its Application in Transparent Polyurethane Coating. *Ind. Eng. Chem. Res.* 2017, 56, 11133−11141.

(14) Valgimigli, L.; Baschieri, A.; Amorati, R. Antioxidant Activity of Nanomaterials. *J. Mater. Chem. B* 2018, 6, 2036−2051.

(15) Richter, A. P.; Brown, J. S.; Bharti, B.; Wang, A.; Gangwal, S.; Houck, K.; Cohen Hubal, E. A.; Paunov, V. N.; Stoyanov, S. D.; Velev, O. D. An Environmentally Benign Antimicrobial Nanoparticle Based on a Silver-Infused Lignin Core. *Nat. Nanotechnol.* 2015, 10, 817−823.

(16) Azam, A.; Ahmed, A. S.; Oves, M.; Khan, M. S.; Habib, S. S.; Adnan, M. Antimicrobial Activity of Metal Oxide Nanoparticles against Gram-Positive and Gram-Negative Bacteria: A Comparative Study. *Int. J. Nanomed.* 2012, 7, 6003−6009.

(17) Zhang, L.; You, T.; Zhou, T.; Zhou, X.; Xu, F. Interconnected Hierarchical Porous Carbon from Lignin-Derived Byproducts of Bioethanol Production for Ultra-High Performance Supercapacitors. *ACS Appl. Mater. Interfaces* 2016, 8, 13918−13925.

(18) Klapiszewski, Ł.; Grząbka-Zasadzińska, A.; Borysiak, S.; Jesionowski, T. Preparation and Characterization of Polypropylene Composites Reinforced by Functional ZnO/Lignin Hybrid Materials. *Polym. Test* 2019, 79, No. 106058.

(19) Wu, W.; Liu, T.; Deng, X.; Sun, Q.; Cao, X.; Feng, Y.; Wang, B.; Roy, V. A. L.; Li, R. K. Y. Ecofriendly UV-Protective Films Based on Poly(Propylene Carbonate) Biocomposites Filled with TiO2 Decorated Lignin. *Int. J. Biol. Macromol.* 2019, 126, 1030−1036.

(20) Shankar, S.; Rhim, J.-W.; Won, K. Preparation of Poly-(Lactide)/Lignin/Silver Nanoparticles Composite Films with UV Light Barrier and Antibacterial Properties. *Int. J. Biol. Macromol.* 2018, 107, 1724−1731.

(21) Yang, W.; Kenny, J. M.; Puglia, D. Structure and Properties of Biodegradable Wheat Gluten Bionanocomposites Containing Lignin Nanoparticles. *Ind. Crops Prod.* 2015, 74, 348−356.

(22) Cho, T.-Y.; Strobl, G. Temperature Dependent Variations in the Lamellar Structure of Poly(L-Lactide). *Polymer* 2006, 47, 1036−1043.

(23) Byun, Y.; Kim, Y. T.; Whiteside, S. Characterization of an Antioxidant Polylactic Acid (PLA) Film Prepared with α-Tocopherol, BHT and Polyethylene Glycol Using Film Cast Extruder. *J. Food Eng.* 2010, 100, 239−244.

(24) Bari, A.; Bloise, N.; Fiorilli, S.; Novajra, G.; Vallet-Regí, M.; Bruni, G.; Torres-Pardo, A.; González-Calbet, J. M.; Visai, L.; Vitale-Brovarone, C. Copper-Containing Mesoporous Bioactive Glass Nanoparticles as Multifunctional Agent for Bone Regeneration. *Acta Biomater.* 2017, 55, 493−504.

(25) Armentano, I.; Fortunati, E.; Latterini, L.; Rinaldi, S.; Saino, E.; Visai, L.; Elisei, F.; Kenny, J. M. Biodegradable PLGA Matrix Nanocomposite with Silver Nanoparticles: Material Properties and Bacteria Activity. *J. Nanostruct. Polym. Nanocompos.* 2010, 6, 110−117.

(26) Yao, Y.; Qin, J.; Cai, Y.; Wei, F.; Lu, F.; Wang, S. Facile Synthesis of Magnetic ZnFe2O4−Reduced Graphene Oxide Hybrid and Its Photo-Fenton-like Behavior under Visible Iradiation. *Environ. Sci. Pollut. Res.* 2014, 21, 7296−7306.

(27) Pang, H.-F.; Xiang, X.; Li, Z.-J.; Fu, Y.-Q.; Zu, X.-T. Hydrothermal Synthesis and Optical Properties of Hexagonal Tungsten Oxide Nanocrystals Assisted by Ammonium Tartrate. *Phys. Status Solidi* 2012, 209, 537−544.

(28) Lucchini, M.; Lizundia, E.; Moser, S.; Niederberger, M.; Nystrom, G. Titania-Cellulose Hybrid Monolith for in-Flow Purification of Water under Solar Illumination. *ACS Appl. Mater. Interfaces* 2018, 10, 29599−29607.

(29) Singh, P. K.; Bishwakarma, H.; Shubham; Das, A. K. Study of Annealing Effects on Ag2O Nanoparticles Generated by Electrochemical Spark Process. *J. Electron. Mater.* 2017, 46, 5715−5727.

(30) Shah, A.; Haq, S.; Rehman, W.; Waseem, M.; Shoukat, S.; Rehman, M. Photocatalytic and Antibacterial Activities of *Paeonia emodi* Mediated Silver Oxide Nanoparticles. *Mater. Res. Express* 2019, 6, No. 45045.

(31) Tang, Z. G.; Black, R. A.; Curran, J. M.; Hunt, J. A.; Rhodes, N. P.; Williams, D. F. Surface Properties and Biocompatibility of Solvent-Cast Poly[ε-Caprolactone] Films. *Biomaterials* 2004, 25, 4741−4748.

(32) Saharudin, K. A.; Sreekantan, S.; Basiron, N.; Khor, L. Y.; Harun, H. N.; Mydin, R. B. S. M. N.; Md Akil, H.; Seeni, A.; Vignesh, K. Bacteriostatic Activity of LLDPE Nanocomposite Embedded with Sol−Gel Synthesized TiO2/ZnO Coupled Oxides at Various Ratios. *Polymers* 2018, 10, No. 878.

(33) Kubacka, A.; Fernández-García, M.; Colón, G. Advanced Nanoarchitectures for Solar Photocatalytic Applications. *Chem. Rev.* 2012, 112, 1555−1614.

(34) Auras, R.; Harte, B.; Selke, S. An Overview of Polylactides as Packaging Materials. *Macromol. Biosci.* 2004, 4, 835−864.

(35) Chandramouleeswaran, S.; Mhaske, S. T.; Kathe, A. A.; Varadarajan, P. V.; Prasad, V.; Vigneshwaran, N. Functional Behaviour of Polypropylene/ZnO-Soluble Starch Nanocomposites. *Nanotechnology* 2007, 18, No. 385702.

(36) Larrañaga, A.; Lizundia, E. A Review on the Thermomechanical Properties and Biodegradation Behaviour of Polyesters. *Eur. Polym. J.* 2019, 121, No. 109296.

(37) Costes, L.; Laoutid, F.; Brohez, S.; Delvosalle, C.; Dubois, P. Phytic Acid−Lignin Combination: A Simple and Efficient Route for Enhancing Thermal and Flame Retardant Properties of Polylactide. *Eur. Polym. J.* **2017**, *94*, 270−285.

(38) Liu, L.; Zachariah, M. R.; Stoliarov, S. I.; Li, J. Enhanced Thermal Decomposition Kinetics of Poly(Lactic Acid) Sacrificial Polymer Catalyzed by Metal Oxide Nanoparticles. *RSC Adv.* **2015**, *5*, 101745−101750.

(39) Lizundia, E.; Larrañaga, A.; Vilas, J. L.; León, L. M. Three-Dimensional Orientation of Poly(l-Lactide) Crystals under Uniaxial Drawing. *RSC Adv.* **2016**, *6*, 11943−11951.

(40) Scherrer, P. Bestimmung Der Größe Und Der Inneren Struktur von Kolloidteilchen Mittels Röntgenstrahlen. *Nachr. Ges. Wiss. Goettingen, Math.-Phys. Kl., Fachgruppe* **1918**, *2*, 98−100.

(41) Jabbarzadeh, A.; Halfina, B. Unravelling the Effects of Size, Volume Fraction and Shape of Nanoparticle Additives on Crystallization of Nanocomposite Polymers. *Nanoscale Adv.* **2019**, *1*, 4704−4721.

(42) Lizundia, E.; Petisco, S.; Sarasua, J.-R. Phase-Structure and Mechanical Properties of Isothermally Melt-and Cold-Crystallized Poly (L-Lactide). *J. Mech. Behav. Biomed. Mater.* **2012**, *17*, 242−251.

(43) Rittigstein, P.; Priestley, R. D.; Broadbelt, L. J.; Torkelson, J. M. Model Polymer Nanocomposites Provide an Understanding of Confinement Effects in Real Nanocomposites. *Nat. Mater.* **2007**, *6*, 278−282.

(44) Weeks, J. J. Melting Temperature and Change of Lamellar Thickness with Time for Bulk Polyethylene. *J. Res. Natl. Bur. Stand., Sect. A* **1963**, *67A*, 441−451.

(45) Lizundia, E.; Fortunati, E.; Dominici, F.; Vilas, J. L.; León, L. M.; Armentano, I.; Torre, L.; Kenny, J. M. PLLA-Grafted Cellulose Nanocrystals: Role of the CNC Content and Grafting on the PLA Bionanocomposite Film Properties. *Carbohydr. Polym.* **2016**, *142*, 105−113.

(46) Lizundia, E.; Sarasua, J. R.; D'Angelo, F.; Orlacchio, A.; Martino, S.; Kenny, J. M.; Armentano, I. Biocompatible Poly(L-Lactide)/MWCNT Nanocomposites: Morphological Characterization, Electrical Properties, and Stem Cell Interaction. *Macromol. Biosci.* **2012**, *12*, 870−881.

(47) Lee, J. H.; Go, A. K.; Oh, S. H.; Lee, K. E.; Yuk, S. H. Tissue Anti-Adhesion Potential of Ibuprofen-Loaded PLLA−PEG Diblock Copolymer Films. *Biomaterials* **2005**, *26*, 671−678.

(48) Moradi, R.; Karimi-Sabet, J.; Shariaty-Niassar, M.; Koochaki, A. M. Preparation and Characterization of Polyvinylidene Fluoride/ Graphene Superhydrophobic Fibrous Films. *Polymers* **2015**, *7*, 1444− 1463.

(49) Lin, F. Y. H.; Li, D.; Neumann, A. W. Effect of Surface Roughness on the Dependence of Contact Angles on Drop Size. *J. Colloid Interface Sci.* **1993**, *159*, 86−95.

(50) Gao, N.; Yan, Y. Modeling Superhydrophobic Contact Angles and Wetting Transition. *J. Bionic Eng.* **2009**, *6*, 335−340.

(51) Kanagesan, S.; Hashim, M.; AB Aziz, S.; Ismail, I.; Tamilselvan, S.; Alitheen, B. N.; Swamy, K. M.; Purna Chandra Rao, B. Evaluation of Antioxidant and Cytotoxicity Activities of Copper Ferrite (CuFe$_2$O$_4$) and Zinc Ferrite (ZnFe$_2$O$_4$) Nanoparticles Synthesized by Sol-Gel Self-Combustion Method. *Appl. Sci.* **2016**, *6*, No. 184.

(52) Das, D.; Nath, B. C.; Phukon, P.; Dolui, S. K. Synthesis and Evaluation of Antioxidant and Antibacterial Behavior of CuO Nanoparticles. *Colloids Surf., B* **2013**, *101*, 430−433.

(53) Yang, W.; Fortunati, E.; Gao, D.; Balestra, G. M.; Giovanale, G.; He, X.; Torre, L.; Kenny, J. M.; Puglia, D. Valorization of Acid Isolated High Yield Lignin Nanoparticles as Innovative Antioxidant/ Antimicrobial Organic Materials. *ACS Sustainable Chem. Eng.* **2018**, *6*, 3502−3514.

(54) Yang, W.; Fortunati, E.; Bertoglio, F.; Owczarek, J. S.; Bruni, G.; Kozanecki, M.; Kenny, J. M.; Torre, L.; Visai, L.; Puglia, D. Polyvinyl Alcohol/Chitosan Hydrogels with Enhanced Antioxidant and Antibacterial Properties Induced by Lignin Nanoparticles. *Carbohydr. Polym.* **2018**, *181*, 275−284.

(55) Liao, C.; Li, Y.; Tjong, C. S. Bactericidal and Cytotoxic Properties of Silver Nanoparticles. *Int. J. Mol. Sci.* **2019**, *20*, No. 449.

(56) Allahverdiyev, A. M.; Abamor, E. S.; Bagirova, M.; Rafailovich, M. Antimicrobial Effects of TiO2 and Ag2O Nanoparticles against Drug-Resistant Bacteria and Leishmania Parasites. *Future Microbiol.* **2011**, *6*, 933−940.

(57) de Toledo, L. d. S.; Rosseto, H. C.; Bruschi, M. L. Iron Oxide Magnetic Nanoparticles as Antimicrobials for Therapeutics. *Pharm. Dev. Technol.* **2018**, *23*, 316−323.

(58) Król, A.; Pomastowski, P.; Rafińska, K.; Railean-Plugaru, V.; Buszewski, B. Zinc Oxide Nanoparticles: Synthesis, Antiseptic Activity and Toxicity Mechanism. *Adv. Colloid Interface Sci.* **2017**, *249*, 37−52.

(59) Sánchez-López, E.; Gomes, D.; Esteruelas, G.; Bonilla, L.; Lopez-Machado, L. A.; Galindo, R.; Cano, A.; Espina, M.; Ettcheto, M.; Camins, A.; et al. Metal-Based Nanoparticles as Antimicrobial Agents: An Overview. *Nanomaterials* **2020**, *10*, No. 292.

(60) Nofar, M.; Sacligil, D.; Carreau, P. J.; Kamal, M. R.; Heuzey, M.-C. Poly(Lactic Acid) Blends: Processing, Properties and Applications. *Int. J. Biol. Macromol.* **2019**, *125*, 307−360.

(61) Hosseini, F.; Rasuli, R.; Jafarian, V. Immobilized WO3nano-particles on Graphene Oxide as a Photo-Induced Antibacterial Agent against UV-ResistantBacillus Pumilus. *J. Phys. D. Appl. Phys.* **2018**, *51*, No. 145403.

(62) Yu, H.-Y.; Yang, X.-Y.; Lu, F.-F.; Chen, G.-Y.; Yao, J.-M. Fabrication of Multifunctional Cellulose Nanocrystals/Poly(Lactic Acid) Nanocomposites with Silver Nanoparticles by Spraying Method. *Carbohydr. Polym.* **2016**, *140*, 209−219.